

# Druggable Hot Spots in the Schistosomiasis Cathepsin B1 Target Identified by Functional and Binding Mode Analysis of Potent Vinyl Sulfone Inhibitors

Adéla Jílková, Petra Rubešová, Jindřich Fanfrlík, Pavla Fajtová, Pavlína Řezáčová, Jiří Brynda, Martin Lepšík, Helena Mertlíková-Kaiserová, Cory D. Emal, Adam R. Renslo, William R. Roush, Martin Horn, Conor R. Caffrey, and Michael Maresš\*



Cite This: *ACS Infect. Dis.* 2021, 7, 1077–1088



Read Online

ACCESS |



Metrics & More



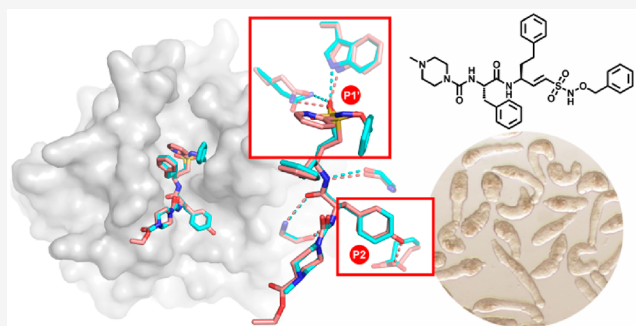
Article Recommendations



Supporting Information

**ABSTRACT:** Schistosomiasis, a parasitic disease caused by blood flukes of the genus *Schistosoma*, is a global health problem with over 200 million people infected. Treatment relies on just one drug, and new chemotherapies are needed. *Schistosoma mansoni* cathepsin B1 (SmCB1) is a critical peptidase for the digestion of host blood proteins and a validated drug target. We screened a library of peptidomimetic vinyl sulfones against SmCB1 and identified the most potent SmCB1 inhibitors reported to date that are active in the subnanomolar range with second order rate constants ( $k_{2nd}$ ) of  $\sim 2 \times 10^5 \text{ M}^{-1} \text{ s}^{-1}$ . High resolution crystal structures of the two best inhibitors in complex with SmCB1 were determined. Quantum chemical calculations of their respective binding modes identified critical hot spot interactions in the S1' and S2 subsites. The most potent inhibitor targets the S1' subsite with an *N*-hydroxysulfonic amide moiety and displays favorable functional properties, including bioactivity against the pathogen, selectivity for SmCB1 over human cathepsin B, and reasonable metabolic stability. Our results provide structural insights for the rational design of next-generation SmCB1 inhibitors as potential drugs to treat schistosomiasis.

**KEYWORDS:** *cathepsin B*, *cysteine peptidase*, *drug target*, *parasite*, *Schistosoma mansoni*, *vinyl sulfone inhibitor*



Schistosomiasis (bilharzia) is a chronic infectious disease caused by trematode blood flukes that infect over 200 million people in tropical and subtropical areas.<sup>1</sup> Of the five species of schistosomes infecting humans, *Schistosoma mansoni* is a major etiological agent of disease in parts of the Middle East, Africa, and South America. Morbidity associated with the disease arises from immunopathological reactions to parasite eggs that accumulate in various tissues.<sup>2</sup> As treatment and control of schistosomiasis rely on just one drug, praziquantel, there is impetus to identify new drugs.<sup>3–5</sup>

Blood proteins are a primary nutritive source for growth, development, and reproduction of the schistosome parasite. In the schistosome gut, a network of peptidases from the cysteine and aspartic protease classes digests host proteins.<sup>6,7</sup> The present research focuses on *S. mansoni* cathepsin B1 (SmCB1), which is a central digestive peptidase because of its high abundance and complex proteolytic activity that comprises both endopeptidase and exopeptidase (peptidyl-dipeptidase) modes of action.<sup>8–10</sup> The SmCB1 structure adopts a classic papain-like fold and contains the occluding loop, a characteristic of cathepsin B-type peptidases,<sup>11</sup> which restricts access to the primed region of the active site; its conformational

flexibility is responsible for the dual cleavage mode of SmCB1.<sup>10</sup> SmCB1 is synthesized as an inactive zymogen and proteolytically converted to a mature enzyme by two alternative activation pathways that are modulated by glycosaminoglycans.<sup>12</sup>

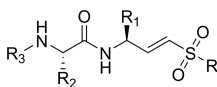
SmCB1 has been validated as a chemotherapeutic target for the cure of schistosomiasis in a murine model using K11777 (*N*-methylpiperazine-phenylalanyl-homophenylalanyl-vinylsulfone-phenyl), a prototype vinyl sulfone inhibitor of cysteine peptidases.<sup>13</sup> Also, the correlation between the severity of the phenotypes induced in *S. mansoni* parasites by vinyl sulfone inhibitors and the potency of inhibition of SmCB1 was demonstrated.<sup>10</sup> Vinyl sulfones were originally investigated for their potential as inhibitors of human cysteine cathepsins<sup>14,15</sup> and later demonstrated to inhibit cysteine peptidases from a

Special Issue: Gut Pathogens

Received: July 14, 2020

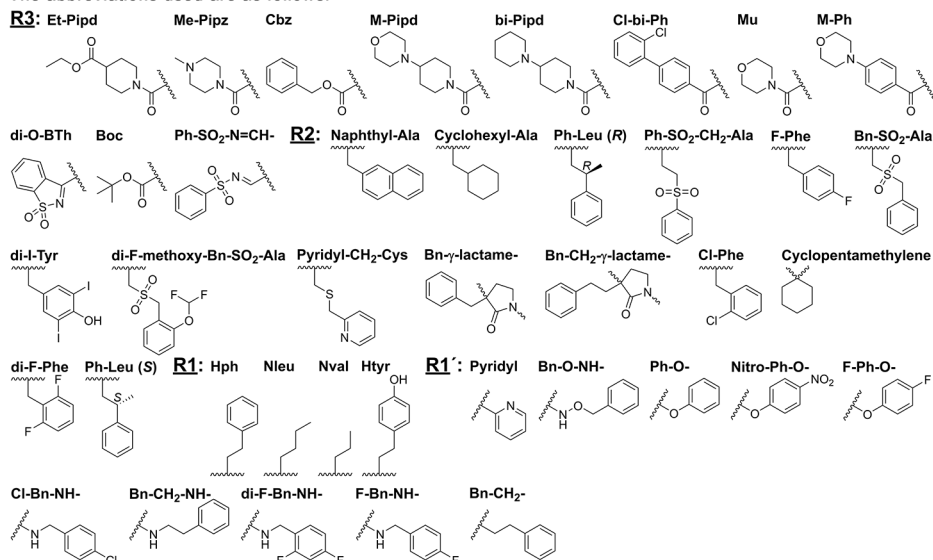
Published: November 11, 2020



Table 1. Inhibition of SmCB1 by Vinyl Sulfone Inhibitors<sup>a</sup>


Compound	Substituent position				Inhibition
Vinyl sulfone	OR3	△R2	□R1	☆R1'	IC <sub>50</sub> (nM)
WRR-391 <sup>b</sup>	Et-Pipd	Tyr	Hph	Pyridyl	0.24 ± 0.03
WRR-286 <sup>b,c</sup>	Me-Pipz	Phe	Hph	★Bn-O-NH-	0.61 ± 0.05
WRR-255	Cbz	Phe	Hph	★Pyridyl	1.50 ± 0.13
WRR-199 <sup>d</sup>	Cbz	Phe	Ala	★Ph-O-	2.55 ± 0.20
CRA-554	M-Pipd	Phe	■Hph	Ph	6.00 ± 0.89
CRA-892	●bi-Pipd	Phe	■Nleu	Ph	7.50 ± 0.58
CRA-553	●M-Pipd	Phe	■Nleu	Ph	13.2 ± 1.3
CRA-547	M-Pipd	▲Naphthyl-Ala	Nva	Ph	39.2 ± 2.2
CRA-446	M-Pipd	▲Phe	■Nva	Ph	44.6 ± 6.1
WRR-258 <sup>d</sup>	Cbz	Phe	Hph	★Nitro-Ph-O-	50.1 ± 4.9
WRR-436	Et-Pipd	Cyclohexyl-Ala	Hph	Ph	72.1 ± 9.1
WRR-206 <sup>c</sup>	Cbz	Phe	Ala	★CH <sub>3</sub> -NH-	93.7 ± 7.3
WRR-353 <sup>d</sup>	Me-Pipz	Phe	Hph	★F-Ph-O-	119 ± 16
CRA-531	Cl-bi-Ph	▲Ph-Leu (R)	Htyr	Ph	155 ± 19
CRA-009	Mu	▲Ph-SO <sub>2</sub> -CH <sub>2</sub> -Ala	Hph	Ph	186 ± 19
CRA-552	M-Pipd	▲F-Phe	Nva	Ph	202 ± 25
CRA-891	Mu	▲Bn-SO <sub>2</sub> -Ala	Hph	Ph	212 ± 10
CRA-373	●H	di-l-Tyr	Nleu	Ph	425 ± 46
CRA-012	Mu	▲di-F-methoxy-Bn-SO <sub>2</sub> -Ala	Hph	Ph	477 ± 43
WRR-201 <sup>c</sup>	Cbz	Phe	Ala	★Cl-Bn-NH-	541 ± 76
CRA-422	M-Ph	di-l-Tyr	Hph	Ph	665 ± 98
WRR-186 <sup>c</sup>	Cbz	Phe	Ala	★Bn-CH <sub>2</sub> -NH-	629 ± 57
WRR-197 <sup>c</sup>	Cbz	Phe	Ala	★di-F-Bn-NH-	1126 ± 120
WRR-196 <sup>c</sup>	Cbz	Phe	Ala	★F-Bn-NH-	1253 ± 173
CRA-393	di-O-BTh	▲Pyridyl-CH <sub>2</sub> -Cys	Nva	Ph	3449 ± 346
CRA-372	●Boc	di-l-Tyr	Nleu	Ph	6252 ± 262
WRR-257	Cbz	Phe	Hph	★Bn-CH <sub>2</sub> -	9517 ± 607
CRA-359	Ph-SO <sub>2</sub> -N=CH-	Cyclohexyl-Ala	Nva	Ph	9990 ± 280
WRR-157	Cbz	▲Bn-γ-lactame-	Hph	Ph	10 <sup>4</sup> - 10 <sup>5</sup>
WRR-188	Cbz	▲Bn-CH <sub>2</sub> -γ-lactame-	Hph	Ph	10 <sup>4</sup> - 10 <sup>5</sup>
CRA-383	di-O-BTh	▲Cl-Phe	Nva	Ph	10 <sup>4</sup> - 10 <sup>5</sup>
CRA-555	Me-Pipz	Cyclopentamethylene	Nva	Ph	n.i.
CRA-845	Cl-bi-Ph	di-F-Phe	Nva	Ph	n.i.
CRA-440	Cl-bi-Ph	▲Ph-Leu (S)	Htyr	Ph	n.i.
<b>Reference compounds</b>					
K11017	Mu	▲Leu	Hph	Ph	1.71 ± 0.13
K11777	Me-Pipz	Phe	Hph	★Ph	2.09 ± 0.08

The abbreviations used are as follows:



<sup>a</sup>The IC<sub>50</sub> values for 34 vinyl sulfone inhibitors were determined in a kinetic activity assay with SmCB1 and the fluorogenic peptide substrate, Cbz-Phe-Arg-AMC, at pH 5.5. The vinyl sulfone structures are defined by the compound core (see scheme) and substituents R3 to R1' (full inhibitor structures are specified in Table S1). Inhibitors are ranked according to their IC<sub>50</sub> values; n.i.: no significant inhibition at 100 μM. Mean values ± SE are given for triplicate measurements. The inhibitors, K11777 and K11017, are indicated as reference compounds.<sup>10</sup> Colored symbols: Homologous compounds that differ only in the substituents in a given position Rx are indicated by the same symbol (identical in color and shape).<sup>b</sup>Crystallographically analyzed in complex with SmCB1. <sup>c</sup>Vinyl sulfonamide. <sup>d</sup>Vinyl sulfonate ester.

variety of protozoan, e.g., *Trypanosoma* and *Plasmodium*, and helminth pathogens, e.g., *Ancylostoma*, providing either a

parasitological cure or a temporary remission of parasitemia.<sup>16–20</sup> As a chemotype, vinyl sulfones have acceptable

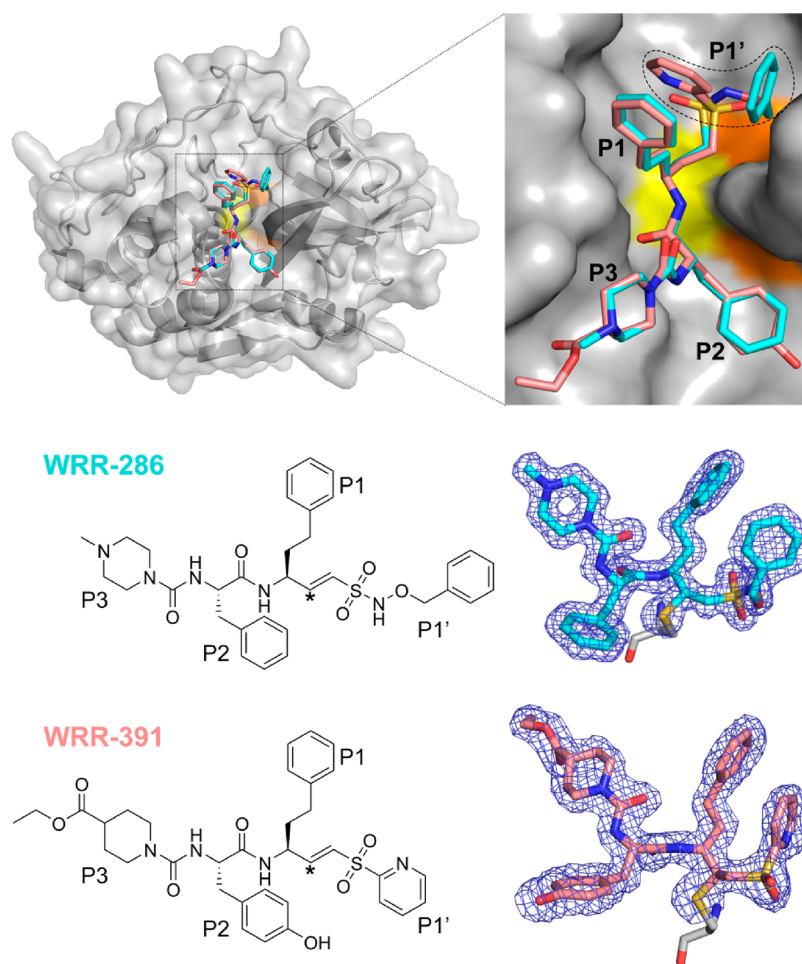


**Figure 1.** Binding mode of subnanomolar vinyl sulfone inhibitors in the SmCB1 active site. Upper panel: The zoomed in view of the SmCB1 active site shows a superposition of the inhibitors WRR-286 and WRR-391 containing the P3 to P1' binding positions (note two different, flipped P1' orientations). SmCB1 is in surface representation; highlighted are the catalytic residues Cys100 (yellow) and His270 and Asn290 (orange). Inhibitors are in stick representation with differently colored carbon atoms (WRR-286, cyan; WRR-391, salmon). Heteroatoms have standard color-coding (O, red; N, blue; S, yellow). Lower panels: Chemical structures of the inhibitors; the C atom forming a covalent bond with the S atom of the catalytic Cys100 is indicated with an asterisk. The  $2F_o - F_c$  electron density maps of the SmCB1-bound inhibitors are contoured at  $1\sigma$ ; the covalently bound catalytic Cys100 is depicted.

pharmacokinetic attributes and *in vivo* safety profiles;<sup>21</sup> the most studied prototype inhibitor K11777 is in preclinical development as an antischistosomal compound.<sup>13,22,23</sup> Therefore, vinyl sulfone inhibitors of SmCB1 represent an attractive option for antischistosomal drug development, and potent and selective derivatives are being pursued. Recently, we determined the crystal structure of SmCB1 in complex with two vinyl sulfone inhibitors, K11777 and K11017 (morpholino urea-leucyl-homophenylalanyl-vinylsulfone-phenyl), effective in nanomolar concentrations.<sup>10</sup> Here, we discover and structurally characterize highly potent subnanomolar inhibitors of SmCB1 and analyze their selectivity and antischistosomal efficiency. Using computational analysis, we provide insight into the energetics of inhibitor binding and identify hot spots for the development of next-generation inhibitor drugs.

## RESULTS

**Mapping of SmCB1 Subsite Specificities with Vinyl Sulfone Peptidomimetics and the Identification of Subnanomolar Inhibitors.** Thirty-four peptidomimetic vinyl sulfone analogs (including vinyl sulfonamides and vinyl sulfonate esters) were explored as potential inhibitors of

SmCB1 to infer the structural requirements of the inhibitor-binding subsites in the enzyme active site cleft. The compound scaffold is defined by positions P3 through P1', and the substitutions were selected to provide a high diversity at P2 and P1' (Table 1). These two positions were recently reported to display large differences in the subsite interaction energy in response to their structural modifications.<sup>10</sup> Homology and structural relationships among the investigated peptidomimetics are presented in Table 1. The compounds were screened *in vitro* against recombinant SmCB1, and their  $IC_{50}$  values were determined using a kinetic inhibition assay with the fluorogenic substrate Cbz-Phe-Arg-AMC.

The P1' position containing various aromatic substituents was critically important in controlling the inhibitor potency. The structure of the aromatic group and the spacer attached to the vinyl sulfone moiety changed the  $IC_{50}$  values in the range of up to 4 orders of magnitude as seen for several groups of homologous derivatives (Table 1). A heterocycle or phenyl with an oxygen-containing linker were favorable P1' substitutions in four inhibitors with  $IC_{50}$  values lower than 3 nM. They also provided two of the best inhibitors that yielded subnanomolar  $IC_{50}$  values, namely, WRR-391 ( $IC_{50} \sim 0.2$  nM)



with a P1' pyridyl and WRR-286 ( $IC_{50} \sim 0.6$  nM) with a P1' phenyl separated by a three-atom linker ( $-NH-O-CH_2-Ph$ ). The P2 position incorporated various aromatic and hydrophobic residues. A change of configuration of the methyl group on C $\gamma$  dramatically decreased the inhibitory potency as shown for CRA-531 and CRA-440. The S2 subsite can accommodate even larger bulky residues such as naphthyl-Ala (CRA-547,  $IC_{50} \sim 40$  nM). In addition, spatially less demanding modifications on aromatic groups can lead to substantial changes, as demonstrated for a para-fluoro modification of Phe, which decreased potency by 1 order of magnitude (CRA-446 vs CRA-552). In contrast, a para-hydroxyl of Tyr residue is in the P2 position of the most potent inhibitor WRR-391 ( $IC_{50} \sim 0.2$  nM).

In summary, screening a library of vinyl sulfone peptidomimetics against SmCB1 identified two inhibitors with subnanomolar  $IC_{50}$  values, which represent the most potent SmCB1 inhibitors reported to date, and structural determinants in P1' and P2 positions that are potentially associated with their high potency.

**Crystal Structures of SmCB1 Complexes with Two Subnanomolar Vinyl Sulfone Inhibitors.** Recombinant SmCB1 was crystallized in complex with two vinyl sulfones identified as subnanomolar inhibitors of SmCB1, namely, WRR-286 and WRR-391. The structures were determined by molecular replacement using the structure of uncomplexed SmCB1 as a model.<sup>12</sup> The final crystallographic models contain SmCB1 residues 70–323 (the SmCB1 zymogen numbering). The SmCB1·WRR-286 complex crystallized in the monoclinic space group  $P2_1$  with three molecules (A to C) in the asymmetric unit and solvent content of  $\sim 47\%$ . The SmCB1·WRR-391 complex crystallized in a trigonal space group  $P3_1$  with three molecules (A to C) in the asymmetric unit and solvent content of  $\sim 46\%$ . The structures were refined using data to resolutions of 1.55 and 1.91 Å for the SmCB1·WRR-286 and SmCB1·WRR-391 complexes, respectively. The electron density used for the modeling of the inhibitors was of high quality in both structures (Figure 1). In both complexes, all three molecules present in the asymmetric unit are very similar. The root-mean-square deviations (RMSDs) for the superposition of the three protein molecule backbones onto each other range from 0.16 to 0.19 and 0.21 to 0.29 Å for SmCB1·WRR-286 and SmCB1·WRR-391, respectively. These values are within the range observed for different crystal structures of identical proteins.<sup>24</sup>

**Binding Mode of Subnanomolar Vinyl Sulfone Inhibitors to SmCB1.** A comparison of SmCB1 in complex with WRR-286 and WRR-391 did not reveal any significant differences in protein structure (backbone RMSD value is 0.33 Å). The active site cleft contains catalytic residues Cys100, His270, and Asn290<sup>10</sup> and has restricted access to the primed region by the occluding loop, a specific 23 amino acid insertion, which is a hallmark of cathepsin B-type peptidases (Phe175 to Pro197). Both inhibitors occupy S1' to S3 subsites making a covalent irreversible bond through the C $\beta$  atom of the vinyl sulfone moiety with the thiol group of Cys100. The chemical structures of WRR-286 and WRR-391 are identical at the P1 position (Hph); however, they differ at the P1' position (Bn–O–NH– and pyridyl, respectively), the P2 position (Phe and Tyr, respectively), and the P3 position (Me-Pipz and Et-Pipd, respectively) (Figure 1, Table 1). In both complexes, there is a set of common interactions between the inhibitor backbone and the active site that involves contacts with Gln94,

Gly98, Cys100, Trp101, Gly143, Gly144, Gly269, His270, and Trp292 (Table S2).

Specific structural determinants of the inhibitors and their interactions in the binding subsites are as follows. Figure 2

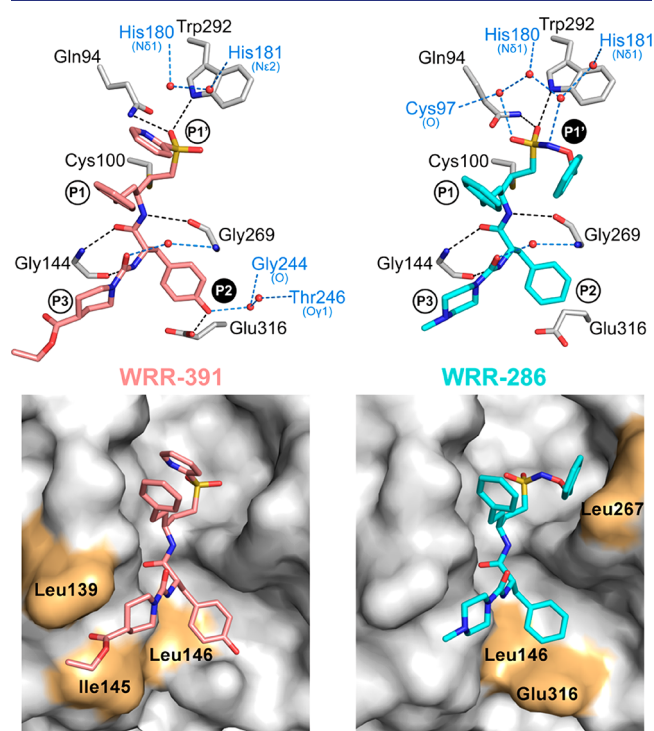


**Figure 2.** Interaction of subnanomolar vinyl sulfone inhibitors with the SmCB1 active site residues. Upper panels: Hydrogen bond network (dashed black lines) between the SmCB1 residues (gray) and inhibitors WRR-391 (salmon) and WRR-286 (cyan). Indirect polar interactions (within 3.2 Å distance and with angle criteria taken into account) via water molecules (red spheres) are shown in dashed blue lines with interacting SmCB1 residues in blue (corresponding atoms are in parentheses). Heteroatoms have a standard color-coding (O, red; N, blue; S, yellow). The P1' to P3 binding positions are indicated, and hot spot positions providing the key interactions are highlighted with black circles. Lower panels: Surface representations of the active site of SmCB1. Highlighted in orange are the SmCB1 residues that form nonpolar interactions with the inhibitors. Inhibitors in stick representation are colored as above.

shows that the S1' subsite is filled by the Bn–O–NH– moiety of WRR-286, whereas the P1' pyridyl moiety of WRR-391 is flipped  $\sim 90^\circ$  out of the active site, as was previously observed for different substituents in this position (Figure S1 and ref 10). The phenyl of WRR-286 is linked by a three-atom linker containing a hydroxylamine unit, which provides greater length and additional degrees of freedom than the pyridyl. Both orientations of the P1' substituents are stabilized by the hydrogen bonds formed between the sulfonyl oxygen of the inhibitors and Gln94 and Trp292 of SmCB1 (Figure 2, Table S2). The P1' benzyl group of WRR-286 is oriented toward residues Val247, Gly269, and Gly268 of the S1' subsite and forms nonpolar interactions with Leu267, while the P1' pyridyl ring of WRR-391 points toward Gln94, Cys97, Gly98, and Ile193 (Figure 2, Table S2). The P1' substituent of WRR-286 forms an extended network of indirect polar interactions via four ordered water molecules at the binding interface, which connect the sulfonyl oxygen and the amine group of the linker with Cys97, and two occluding loop residues His180 and

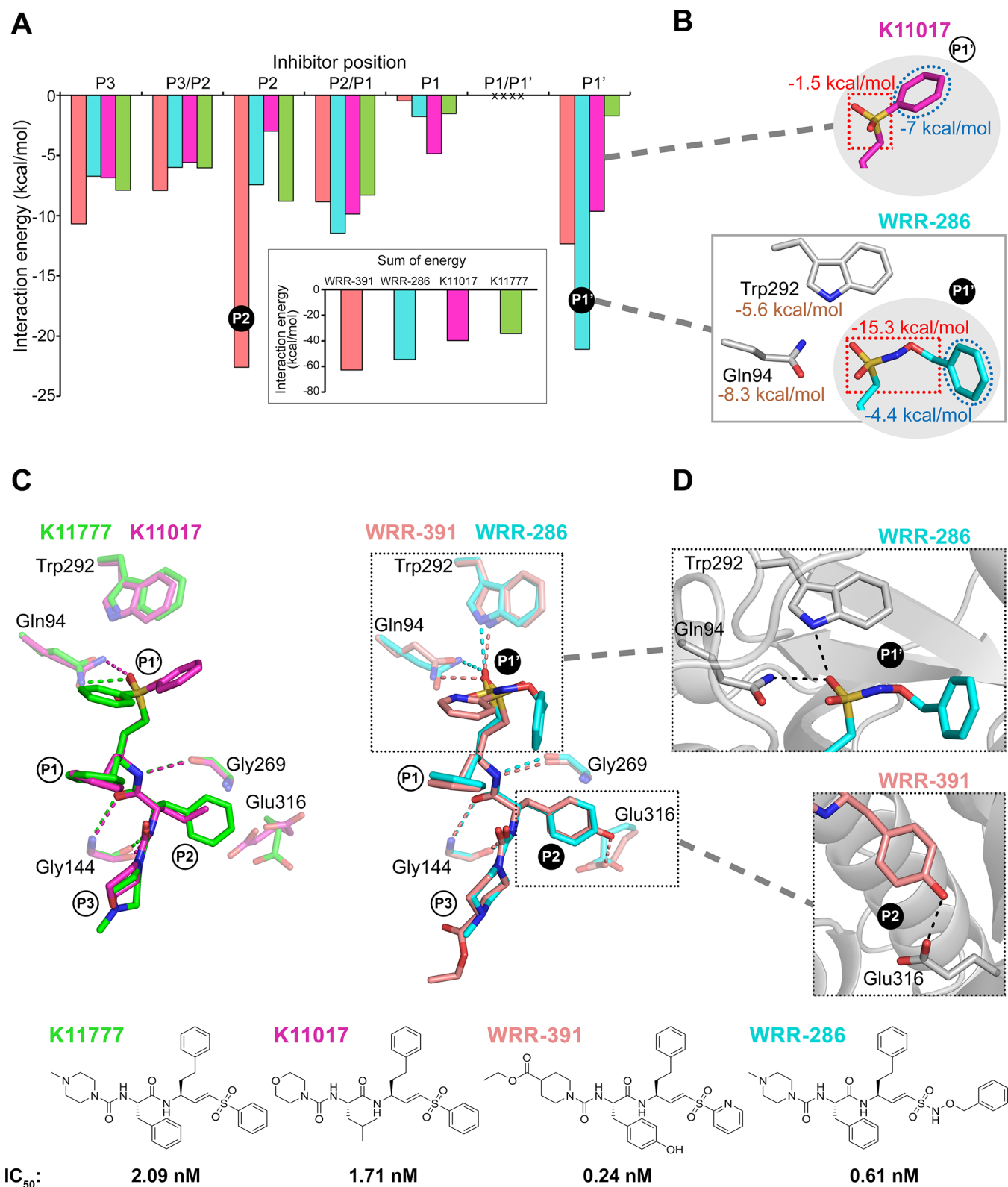


**Figure 3.** Two hot spots confer subnanomolar potency to vinyl sulfone inhibitors of SmCB1. (A) Subsite interaction “free” energies between the inhibitors and SmCB1. The interaction “free” energy was determined using quantum chemical calculations on the crystallographic complexes of the subnanomolar inhibitors, WRR-391 (salmon) and WRR-286 (cyan), and the nanomolar inhibitors, K11017 (magenta, PDB code 3S3Q) and K11777 (green, PDB code 3S3R). The inhibitor structures were fragmented into the side-chain segments (P3 to P1') and main-chain segments (P<sub>i</sub>/P<sub>(i-1)</sub>) connecting the side-chain segments. The P1/P1' segment forming a covalent bond with the catalytic Cys100 was not calculated. Inset: The total interaction “free” energy for each inhibitor calculated as a sum of the individual contributions of the inhibitor segments. Hot spot positions providing the key interactions between the inhibitors and SmCB1 are marked with black circles. (B) Contributing interaction “free” energies in the P1' position. Lower panel: The hot spot P1' substituent of WRR-286 (cyan) was fragmented into the  $-\text{CH}_2-\text{SO}_2-\text{NH}-\text{O}-\text{CH}_2-$  moiety (red box) and the phenyl ring (blue circle). Their interaction “free” energies with SmCB1 determined using quantum chemical calculations

Figure 3. continued

are indicated (data in red and blue). Interaction “free” energies of the SmCB1 residues Trp292 and Gln94 were calculated using the virtual glycine scan (data in brown). Upper panel: For comparison, K11017 (magenta) with a homologous P1' substituent was fragmented into the  $-\text{CH}_2-\text{SO}_2-$  segment (red box) and the phenyl ring (blue circle), and their interaction “free” energies were analyzed. (C) A superposition of inhibitors bound to SmCB1. Left panel: inhibitors K11777 (green, PDB code 3S3R) and K11017 (magenta, PDB code 3S3Q). Right panel: inhibitors WRR-391 (salmon) and WRR-286 (cyan). Hydrogen bonds formed between the inhibitors and SmCB1 residues (transparent) are shown as dashed lines. Heteroatoms have a standard color-coding (O, red; N, blue; S, yellow). Hot spot positions and their interactions are boxed and marked with black circles. (D) A detailed view of two hot spots in the subnanomolar inhibitors. Upper panel: The P1' hot spot of the inhibitor WRR-286 (cyan) involves a hydrogen bonding between the sulfonyl oxygen and Trp292 and Gln94 of SmCB1. Lower panel: The P2 hot spot of the inhibitor WRR-391 (salmon) involves a hydrogen bond between the Tyr hydroxyl and the Glu316 carboxylate of SmCB1. SmCB1 residues are shown in gray and hydrogen bonds, as dashed black lines; heteroatoms have a standard color-coding.

	k <sub>2nd</sub> (M <sup>-1</sup> s <sup>-1</sup> )		rate constant protease	Antischistosomal effect					
	SmCB1	HuCB		1 μM		10 μM		inhibitor concentration hours	
	24	48	72	24	48	72	24	48	72
WRR-391	208 414	152 806		0	0	0	0	0	4
WRR-286	199 876	33 618		0	0	4	0	4	4
K11777	88 851	12 602		0	0	3	0	1	3
				0	1	2	3	4	severity score

**Figure 4.** Selectivity and bioactivity of subnanomolar inhibitors WRR-391 and WRR-286. (A) Sensitivity of SmCB1 and its human ortholog cathepsin B (HuCB) to inhibitors. The second order rate constants were measured in a kinetic activity assay with the fluorogenic peptide substrate Cbz–Phe–Arg–AMC at pH 5.5. Mean values are given for triplicate measurements (SE values were within 10% of the mean). (B) Phenotypic alterations of newly transformed schistosomula of *S. mansoni* induced by the inhibitors applied at 1 and 10 μM concentrations. Resulting phenotypes observed at three time points were graded by the severity score ranging from 0 to 4, with 4 being the most severe (see Figure S2A,B). The prototype vinyl sulfone inhibitor K11777 was used as a reference compound in (A) and (B).

His181 (Figure 2). In contrast, only two water molecules are in the S1' subsite of the SmCB1·WRR-391 complex interacting with residues His180 and His181 with the closest distance to the inhibitor of approximately 3.4 Å (Figure 2). The S1 subsite of SmCB1 binds the Hph residue in both inhibitors by a similar network of contacts (Table S2). In WRR-391, the phenyl ring of Hph forms an aromatic stacking interaction with the P1' pyridyl group with approximately 4 Å separation. The bottom of the S2 subsite contains Glu316. It tightly anchors Tyr in the P2 position of WRR-391 through a hydrogen bond between the phenolic hydroxyl and carboxylate oxygen with a distance of 2.38 Å. This interaction is absent for WRR-286 with the Phe residue in P2, and Glu316 points out of the S2 pocket in the inhibitor complex (Figure 2). The S3 subsite of the SmCB1 active site is wide and generally hydrophobic and accommodates the terminal groups Et-Pipd and Me-Pipz as the P3 substituents of WRR-391 and WRR-286, respectively. In WRR-391, the heterocyclic group extended with the ethoxycarbonyl group provides additional contacts (including nonpolar interactions) with Gly138, Ile145, and Leu139 (Table S2, Figure 2).

**Identification of Inhibitor Hot Spots by Computational Analysis.** Quantum chemical calculations on the crystallographic complexes were carried out to determine the interaction “free” energy of the WRR-286 and WRR-391 inhibitors in the subsites of SmCB1. Figure 3A and Table S3 show the noncovalent interaction “free” energies of the individual side-chain and main-chain segments in P3 to P1' positions. In addition, both subnanomolar inhibitors, WRR-286 and WRR-391, are compared with two nanomolar inhibitors, K11017 and K11777, for which their complexes with SmCB1 were structurally characterized previously.<sup>10</sup> The analysis revealed rather smaller favorable contributions (up to

–13 kcal/mol) at individual positions of all the inhibitors and two large favorable contributions exceeding –20 kcal/mol. The dominant interactions come from the side chains of P2 in WRR-391 and P1' in WRR-286. Due to their contributions, the total binding energies of the subnanomolar inhibitors shifted to more negative values than those calculated for nanomolar inhibitors (Figure 3A, Table S3). These two positions represent “hot spots” in inhibitor structures that provided specific key contributions to the subnanomolar inhibition of SmCB1.

In the SmCB1·WRR-391 complex, the P2 hot spot interaction (–22.6 kcal/mol) is formed by the Tyr substituent (Figure 3A, Table S3). It makes a specific hydrogen bonding with Glu316 of SmCB1, which cannot be established by the other inhibitors WRR-286, K11777, and K11017, containing Phe or Leu at the P2 position (Figures 3C,D and S1). In the SmCB1·WRR-286 complex, the P1' hot spot interaction (–21.1 kcal/mol) is formed by the  $-\text{CH}_2-\text{SO}_2-\text{NH}-\text{O}-\text{CH}_2-\text{Ph}$  segment (Figure 3A, Table S3). It was decomposed into two fragments, and their interaction “free” energies were calculated to dissect the binding contributions. We demonstrated that the more favorable interaction comes from the  $-\text{CH}_2-\text{SO}_2-\text{NH}-\text{O}-\text{CH}_2-$  moiety (–15.3 kcal/mol) than from the Ph ring (–4.4 kcal/mol) (Figure 3B); their sum closely matches the interaction “free” energy calculated for the whole segment. Furthermore, the interaction “free” energy contributions of the relevant SmCB1 residues in the S1' pocket were evaluated using the virtual glycine scan. This showed that the side chains of the Gln94 and Trp292 residues, forming hydrogen bonds with the sulfonyl oxygen of P1', contribute –8.3 and –5.6 kcal/mol, respectively (Figure 3B). In total, these values represent a major part of the binding energy by the  $-\text{CH}_2-\text{SO}_2-\text{NH}-\text{O}-\text{CH}_2-$  moiety. Thus, Gln94 and



Trp292 are responsible for the key enzyme interactions with the P1' hot spot of WRR-286 (Figure 3C,D).

**Selectivity, Bioactivity, and Plasma-Stability Profiling Identifies WRR-286 as a Lead Molecule.** The *in vitro* potency of subnanomolar inhibitors WRR-286 and WRR-391 was analyzed in detail by the second order rate constant ( $k_{2nd}$ ). This allowed for direct comparison of the inhibition of SmCB1 and human cathepsin B to explore the selectivity of the investigated compounds (Figure 4A). We demonstrated that both inhibitors display a certain degree of selectivity toward SmCB1. WRR-286 was substantially more selective than WRR-391 with selectivity ratios of about 6.0 ( $k_{2nd}$  values of 199 876  $M^{-1} s^{-1}$  for SmCB1 to 33 618  $M^{-1} s^{-1}$  for human enzyme) and 1.4 (208 414 to 152 806  $M^{-1} s^{-1}$ ), respectively. The selectivity of WRR-286 is comparable with that of the prototype vinyl sulfone inhibitor K11777 with the selectivity ratio of about 7.1 (88 851 to 12 602  $M^{-1} s^{-1}$ ), but it possesses weaker potency.

The subnanomolar inhibitors were next tested for bioactivity against *S. mansoni* newly transformed schistosomula (NTS), the postinvasive parasite stage that feeds on host blood. The NTS were exposed to 1 and 10  $\mu M$  inhibitors, and the resulting phenotypes were graded 0 through 4 from the least to the most severe (Figure 4B).<sup>25,26</sup> We found that both inhibitors differed in their bioactivities (Figure 4B). WRR-286 was the more potent and caused parasite degeneration with the maximum severity score of 4 at 1  $\mu M$  after 72 h, whereas WRR-391 generated a similar effect at 10  $\mu M$ . Importantly, WRR-286 was also more effective than the prototype vinyl sulfone inhibitor K11777, which has been previously evaluated as an antischistosomal agent in *ex vivo* and *in vivo* studies.<sup>10,13</sup> The investigated inhibitors were also tested for their cytotoxicity against four human cell lines over 72 h. Both displayed low cytotoxicity at the same concentrations used in the NTS assay (Figure S2C), indicating that the observed phenotypic changes were specific to the parasite.

Finally, we evaluated the metabolic stability of the inhibitors in human plasma *in vitro*. The stability was expressed as the percentage of parental compound remaining in plasma after 30 min of incubation. WRR-286 and K11777 displayed a high plasma stability with the percentage of remaining compound of 107% and 88%, respectively, which is in contrast to the weaker stability of WRR-391 with just 54% remaining (Figure S2D).

To conclude, the inhibitor WRR-286 was identified as a lead molecule based on inhibition potency, selectivity to the SmCB1 target, and antischistosomal activity.

## DISCUSSION

SmCB1 is a critical digestive peptidase in the gut of the flatworm parasite *S. mansoni*<sup>6,9,27</sup> and a target for antischistosomal drugs.<sup>13,28</sup> Peptidomimetic protease inhibitors with a vinyl sulfone warhead are potent SmCB1 binders and antischistosomal<sup>10</sup> with superior functional properties compared to other tested inhibitor chemotypes.<sup>29,30</sup> In this study, we provide the first structural characterization of inhibitors effective against SmCB1 in a subnanomolar range and identify the hot spots underpinning that potency.

Two SmCB1 inhibitors, WRR-286 and WRR-391, with  $IC_{50}$  values of 0.61 and 0.24 nM were selected from a vinyl sulfone library, and their binding mode was determined by crystallographic analysis in complex with SmCB1 and by quantum chemical calculations. On the basis of these, we defined two critical hot spot positions in these inhibitors targeting the S2 and S1' subsites of SmCB1, namely, the P2 substituent of

WRR-391 and P1' substituent of WRR-286. The active site of cathepsin B and other papain-family cysteine peptidases comprises five subsites from S3 to S2'. Three of them, subsites S2, S1, and S1', are shaped to allow extensive binding of the substrate residues by the main-chain and side-chain interactions; the deep pocket of the S2 subsite is typically a key determinant of specificity.<sup>31,32</sup> The S2 subsite of SmCB1 and human cathepsin B contains a Glu residue (Glu316 in SmCB1). It tolerates Arg at P2 in the substrates, in contrast to many other family members.<sup>31</sup> Previously, we demonstrated the functionality of the P2 Arg in an SmCB1 inhibitor; however, it did not provide better potency over the preferential Phe substituent<sup>10</sup> in agreement with the specificity demonstrated for this position using fluorogenic peptide substrates.<sup>8</sup> Here, we show that Tyr in the P2 position of WRR-391 is a hot spot that forms a hydrogen bond with Glu316, thereby allowing an energetically favorable interaction with SmCB1. This interaction is absent in the structurally characterized SmCB1 complexes of WRR-286, K11777, and K11017 inhibitors that contain Phe or Leu residues at P2 (Figure 3). In these complexes, Glu316 is conformationally highly flexible, and this is similar to the acidic S2 residues found in the *Trypanosoma* and *Plasmodium* cathepsin L-type peptidases complexed with vinyl sulfones.<sup>33</sup>

The critical structural segment within the P1' hot spot of WRR-286 was identified using quantum chemical calculations and decomposition of binding energy. The more favorable interaction comes from the  $-CH_2-SO_2-NH-O-CH_2-$  moiety ( $-15.3$  kcal/mol) than from the phenyl ring ( $-4.4$  kcal/mol) (Figure 3B). The binding contributions in P1' were compared with those in the nanomolar inhibitor K11017 for which the P1' substituent has a related structure and conformation. The distribution of binding energy is reversed compared to WRR-286 since the  $-CH_2-SO_2-$  moiety ( $-1.5$  kcal/mol) contributes less than the phenyl ring ( $-7$  kcal/mol) (Figure 3B). Whereas the contributions of the phenyl ring are rather comparable, the contributions of the "sulfone linker" moiety differ by 1 order of magnitude. This analysis suggests that the extended three-atom linker is critical to the P1' hot spot and its interactions with the S1' pocket. The linker may control the orientation of the sulfone group forming two hydrogen bonds in WRR-286 (with Gln94 and Trp292) but only one hydrogen bond in K11017 (with Gln94) (Figure 3C). The hydrogen bond to Trp292 (an important residue for positioning the enzyme catalytic machinery<sup>34</sup>) is present in both WRR-286 and WRR-391 but absent in the less potent K11017 and K11777. Our conclusions on the regulatory role of a P1' linker are in line with the findings previously reported for the inhibition of the trypanosomal peptidase, cruzain.<sup>34</sup> Future inhibitor designs incorporating the P1' hot spot may be combined with the extending interactions into the S2' subsite, which provides a high binding energy contribution and specificity, as demonstrated for the epoxide inhibitor, CA074.<sup>10</sup>

We investigated and compared the relevant functional properties of WRR-286 and WRR-391. First, we evaluated the inhibitory potency toward SmCB1 and human cathepsin B using second order rate constants. This demonstrated that WRR-286 displays a substantial degree of selectivity for SmCB1 over the human enzyme in contrast to the weaker selectivity of WRR-391. Second, against *S. mansoni* in culture, WRR-286 had a strong degenerative effect, whereas WRR-391 was less potent. Third, WRR-286 has a better plasma stability compared to WRR-391.

In conclusion, our analysis of the functional properties of a set of vinyl sulfone peptidomimetic inhibitors has identified the subnanomolar SmCB1 inhibitor WRR-286 as a lead molecule for further optimization. The crystallographic and quantum chemical insights into the binding and structure–activity relationships of vinyl sulfone inhibitors of the SmCB1 target will facilitate a further rational design of potential anti-schistosomal drugs.

## METHODS

**Ethical Statement.** Maintenance of the *S. mansoni* life cycle is as described<sup>13,35</sup> and involves the use of hamsters as a definitive host. The use of hamsters for this purpose has been reviewed and approved by UC San Diego's Institutional Animal Care and Use Committee (IACUC). The protocol complies with United States federal regulations regarding the care and use of laboratory animals: Public Law 99-158, the Health Research Extension Act, and Public Law 99-198, the Animal Welfare Act, which is regulated by USDA, APHIS, CFR, Title 9, Parts 1, 2, and 3.

**Materials.** Vinyl sulfone inhibitors (Tables 1 and S1) were selected from the Collaborative Drug Discovery database (<http://www.collaborativedrug.com>) and synthesized and purified as described previously.<sup>14,34,36–41</sup> The purity of the compounds was assessed by an analytical Agilent 1200 Series HPLC with a C18 column (Phenomenex, 5  $\mu$ m, 250  $\times$  4.6 mm) using a trifluoroacetic acid/acetonitrile mobile phase system with a linear gradient of acetonitrile. The compounds were of at least 95% purity. All compounds passed the PAINS filter using a false positive remover.<sup>42</sup> Human cathepsin B (HuCB) was obtained from Calbiochem.

**Production and Purification of Recombinant SmCB1.** A nonglycosylated mutant of the SmCB1 zymogen (Uniprot accession Q8MNY2) was expressed in the yeast *Pichia pastoris* (strain X-33), activated by *S. mansoni* legumain, and purified as described previously.<sup>43,44</sup> All purification steps were performed under reducing conditions in the presence of 2 mM dithiothreitol and 1 mM EDTA to prevent the active site cysteine from oxidation.

**Preparation of SmCB1–Inhibitor Complexes.** The activated SmCB1 was incubated with a 5-fold molar excess of the inhibitor in 0.1 M sodium acetate, 20 mM cysteine, and 1 mM EDTA, pH 5.5, under an argon atmosphere (10 h, 18 °C). The enzyme inhibition was monitored with Cbz–Phe–Arg–AMC substrate. The complex was chromatographed on an FPLC Mono S column,<sup>43,44</sup> concentrated, and buffer-exchanged into 2.5 mM sodium acetate, pH 5.5, using Amicon Ultracel-10k centrifugal units (Millipore).

**Protein Crystallization and Data Collection.** Crystals were grown by vapor diffusion in hanging drops at 20 °C. The ratio of protein to reservoir solution in drops was 1:1 and 4:1 for the SmCB1·WRR-286 and SmCB1·WRR-391 complexes, respectively. Drops were equilibrated over 1 mL of reservoir solution consisting of 0.2 M ammonium acetate, 0.1 M sodium citrate, and 30% PEG 1500, pH 6.1, for SmCB1·WRR-286 complex and 0.14 M ammonium acetate, 0.07 M sodium citrate, and 21% PEG 400, pH 6.1, for SmCB1·WRR-391 complex. Protein concentrations of the stock solutions were 5.0 and 3.4 mg/mL for the SmCB1·WRR-286 and SmCB1·WRR-391 complexes, respectively. The crystals were flash-cooled by plunging into liquid nitrogen without additional cryoprotection. Diffraction data from the crystal of SmCB1·WRR-286 were collected at 100 K on MX 14.1 operated by the

Helmholtz-Zentrum Berlin at the BESSY II electron storage ring in Berlin-Adlershof, Germany;<sup>45</sup> data from the crystal of SmCB1·WRR-391 were collected at 100 K at the X-ray diffraction station MicroMax-007 HF Microfocus with a Pilatus 300 K detector. All diffraction data were processed using the XDS suite of programs.<sup>46</sup> Crystal parameters and data collection statistics are given in Table 2.

**Table 2. X-ray Data Collection and Refinement Statistics**

SmCB1–inhibitor complex <sup>a</sup>	SmCB1·WRR-286	SmCB1·WRR-391
Data Collection Statistics		
wavelength (Å)	0.918	1.542
temperature (K)	100	100
space group	P2 <sub>1</sub>	P3 <sub>1</sub>
a, b, c (Å)	65.48, 78.07, 77.66	82.39, 82.39, 99.39
$\alpha$ , $\beta$ , $\gamma$ (deg)	90.00, 91.24, 90.00	90, 90, 120
resolution (Å)	39.04–1.55 (1.64–1.55)	38.06–1.91 (1.95–1.91)
number of unique reflections	112 101 (17 919)	52 771 (21 49)
redundancy	3.3 (3.3)	2.8 (1.4)
completeness (%)	98.9 (98.1)	89.5 (48.7)
R <sub>merge</sub> <sup>b</sup> (%)	6.1 (70.7)	7.8 (79.9)
average I/ $\sigma$ (I)	11.81 (1.76)	9.72 (0.68)
CC <sub>1/2</sub> <sup>c</sup> (%)	99.8 (69.0)	99.6 (40.0)
Wilson B (Å <sup>2</sup> )	26.83	31.10
Refinement Statistics		
resolution range (Å)	39.04–1.55 (1.59–1.55)	38.06–1.91 (1.96–1.91)
number of reflections in working set	110 979 (8008)	51 402 (2072)
number of reflections in test set	1121 (80)	1367 (60)
R value <sup>d</sup> (%)	16.2 (32.3)	16.7 (28.2)
R <sub>free</sub> value <sup>e</sup> (%)	20.3 (33.5)	18.6 (29.8)
number of molecules in AU <sup>f</sup>	3	3
number of atoms in AU <sup>f</sup> protein/inhibitor/solvent	6120/132/896	6007/138/447
average ADP <sup>g</sup> for protein/inhibitor/solvent (Å <sup>2</sup> )	26.7/19.9/33.3	29.7/22.8/30.9
RMSD bond length (Å)	0.015	0.010
RMSD bond angle (deg)	1.604	1.409
Ramachandran plot statistics <sup>h</sup>		
favored regions (%)	96.3	93.4
allowed regions (%)	3.7	6.6
PDB code	SOGR	SOGQ

<sup>a</sup>Numbers in parentheses refer to the highest-resolution shell. <sup>b</sup>R<sub>merge</sub> =  $100 \sum_{hkl} \sum_i |I_i(hkl) - \langle I(hkl) \rangle| / \sum_{hkl} \sum_i I_i(hkl)$ , where  $I_i(hkl)$  is an individual intensity of the  $i^{\text{th}}$  observation of reflection  $hkl$  and  $\langle I(hkl) \rangle$  is the average intensity of reflection  $hkl$  with summation over all data. <sup>c</sup>CC<sub>1/2</sub> is the percentage of correlation between intensities from random half-datasets.<sup>47</sup> <sup>d</sup>R value =  $\|F_o\| - \|F_c\| / \|F_o\|$ , where  $F_o$  and  $F_c$  are the observed and calculated structure factors, respectively. <sup>e</sup>R<sub>free</sub> is equivalent to the R value but is calculated for up to 5% of the reflections chosen at random and omitted from the refinement process.<sup>48</sup> <sup>f</sup>AU, asymmetric unit. <sup>g</sup>ADP, atomic displacement parameter, formally B-factor. <sup>h</sup>As determined by Molprobit.<sup>49</sup>

## Structure Determination, Refinement, and Analysis.

The structures of SmCB1·WRR-286 and SmCB1·WRR-391 were determined by molecular replacement with the program Molrep<sup>50</sup> using the structure of the mature SmCB1 (PDB code 4I07<sup>12</sup>) as the search model. Model refinement was carried out using the program REFMAC 5.2<sup>51</sup> from the CCP4 package,<sup>52</sup> interspersed with manual adjustments using Coot.<sup>53</sup> The



geometric restraints for ligands were constructed by the program Libcheck<sup>52</sup> using inhibitors optimized by the method DFT-D3/B3LYP/DZVP<sup>54</sup> combined with the COSMO<sup>55</sup> implicit solvent model. The optimization was performed by the Turbomole7.0<sup>56</sup> and Cuby4<sup>57</sup> programs. The final steps of the isotropic ADP refinement of SmCB1-WRR-286 included TLS parametrization.<sup>58</sup> For the SmCB1-WRR-391 complex, the merohedric twinning was detected and was taken into the account during rebuilding and refinement. The quality of the final models was validated with Molprobit.<sup>49</sup> The final refinement statistics are given in Table 2. The structures were analyzed using the program CONTACT;<sup>52</sup> the nonpolar interactions were determined using the program PLIP<sup>59</sup> and represent contacts with a 4.0 Å distance cutoff between two hydrophobic atoms defined as carbon atoms having carbon or hydrogen atoms as neighbors. All figures showing structural representations were prepared with the PyMOL Molecular Graphics System, Version 1.4 Schrödinger, LLC.

**Interaction “Free” Energy Calculations.** For all calculations, chain A of the crystal structures and conformation A of the residues with alternative conformations were used. Hydrogen atoms were added to the studied crystallographic complexes and optimized using the AMBER10 software.<sup>60</sup> Further optimization of the inhibitor in the active site was carried out using the corrected semiempirical quantum chemical PM6-D3H4 method<sup>61</sup> including the implicit COSMO<sup>55</sup> model of water. The bridging crystallographic water molecules around the inhibitors were considered (namely, waters 515, 519, 558, 735, and 763 for the SmCB1-WRR-286 complex and waters 1137, 1160, 1171, 1182, 1194, 1230, and 1243 for the SmCB1-WRR-391 complex). Residues within 6 Å of the inhibitors were allowed to move during optimization, whereas the rest of the system was frozen. PM6-D3H4 calculations were performed using the MOPAC2016<sup>62</sup> and Cuby4<sup>57</sup> programs. The H4 correction was not used for oxygen atoms bound to sulfur in the sulfone group. A revised version of the repulsive term of the D3 dispersion correction was used.<sup>63</sup> Besides using up-to-date corrections in the semiempirical method, the applied methodology was the same as reported previously.<sup>10</sup>

Interaction “free” energies of the individual subsites were computed on the optimized complexes. The inhibitor structures were fragmented into the P3 to P1’ segments with separated side chains and main chains and capped by hydrogen atoms. The reactive centers of the inhibitors originating from the vinyl moieties (located between P1 and P1’) as well as the catalytic Cys100 that form the covalent linkage were not considered in the single point energy calculations. The subsite interaction “free” energies were obtained as the difference between the energy of the fragment noncovalently bonded to the enzyme and the sum of the energies of the enzyme and the inhibitor fragment calculated separately. The PM6-D3H4/COSMO quantum chemical method was applied as described above.

The P1’ segments of the WRR-286 and K11017 inhibitors in complex with SmCB1 were further fragmented into the phenyl ring and the  $-\text{CH}_2-\text{SO}_2-\text{NH}-\text{O}-\text{CH}_2-$  or  $-\text{CH}_2-\text{SO}_2-$  segments, respectively. The fragments were capped by hydrogens, except for the sulfone group of the  $-\text{CH}_2-\text{SO}_2-$  segment which was capped by methyl, and their subsite interaction “free” energies were calculated. The contributions of Trp292 and Gln94 residues to the binding of WRR-286 and K11017 were examined by virtual glycine scanning.<sup>64,65</sup> The

energy contributions of individual residues to the binding were calculated as the difference between the original interaction “free” energy at the PM6-D3H4/COSMO level with the wild type amino acid and with the mutated glycine residue. We considered whole inhibitors, but the side chain of catalytic Cys100 was omitted in the glycine scan calculations.

The analyzed structures of WRR-286 and WRR-391 in complex with SmCB1 provide novel insights into the conformational variability of the P1’ substituents (Figure S1) and their contribution to SmCB1 inhibition (Figure S3 and ref 66).

**Inhibition Assays.** Inhibition measurements were performed in triplicates in 96-well microplates (100  $\mu\text{L}$  assay volume) at 37 °C. To determine IC<sub>50</sub> values, SmCB1 (20 pM) was preincubated with inhibitor (0–100  $\mu\text{M}$ ) in 0.1 M sodium acetate, 2.5 mM dithiothreitol, and 0.1% PEG 1500, pH 5.5, for 5 min followed by the addition of fluorogenic substrate Cbz–Phe–Arg–AMC (20  $\mu\text{M}$ ).<sup>10</sup> The kinetics of product release was continuously monitored in an Infinite M1000 microplate reader (Tecan) at excitation and emission wavelengths of 360 and 465 nm, respectively. The IC<sub>50</sub> values were determined by nonlinear regression using GraFit software. To determine the inhibition constant  $k_{2nd}$ , the enzyme (40 pM SmCB1 or 60 pM HuCB) was added to a mixture of the fluorogenic substrate Cbz–Phe–Arg–AMC (20  $\mu\text{M}$  for SmCB1 and 33  $\mu\text{M}$  for HuCB) and an inhibitor (0–1  $\mu\text{M}$ ) in the assay buffer under assay conditions as above. The hydrolysis of substrate was monitored for 30 min in a microplate reader as described above. An observed rate constant,  $k_{obs}$ , was calculated at each inhibitor concentration by fitting the progress curve to the equation  $P = v_i/k_{obs}(1 - e^{-k_{obs}t})$ , where  $P$  is the product formation,  $v_i$  is the initial velocity, and  $t$  is the reaction time. For both enzymes,  $k_{obs}$  varied linearly with the inhibitor concentration showing that the dependence of  $k_{obs}$  on the inhibitor concentration is nonsaturating. This kinetic mechanism does not allow the determination of the individual  $k_{inact}$  and  $K_i$  parameters. The second order rate constant,  $k_{2nd}$ , was determined by fitting to the linear equation  $k_{obs} = (k_{2nd}[I])/(1 + [S]/K_M)$ , where  $[S]$  is the substrate concentration,  $[I]$  is the inhibitor concentration, and  $K_M$  is the Michaelis–Menten constant.  $K_M$  values determined for SmCB1 and HuCB were 25 and 38  $\mu\text{M}$ , respectively. In all assay systems, the final concentration of dimethyl sulfoxide did not exceed 1.5%.

**Parasite Assay and Phenotype Scoring.** Newly transformed schistosomula (NTS) of *S. mansoni* were prepared by mechanically transforming infective larvae (cercariae) as described previously.<sup>67</sup> NTS (200–300 parasites) were incubated in 200  $\mu\text{L}$  of Basch Medium 169<sup>68</sup> containing 5% heat-inactivated fetal bovine serum, 100 U/mL penicillin, and 100  $\mu\text{g}/\text{mL}$  streptomycin at 5% CO<sub>2</sub> and 37 °C.<sup>67,69</sup> Inhibitors were added at final concentrations of 1 or 10  $\mu\text{M}$  (0.5% dimethyl sulfoxide final),<sup>10,70</sup> and changes in phenotypes were observed every 24 h for 72 h. We use single word or phrase “descriptors”<sup>35</sup> to record changes in movement, shape, and translucence (Figure S2). These descriptors are then converted into an ordinal “severity score” system from 0 (no effect) to 4 (maximum effect), which allows for a relative comparison of compound effects, as described previously.<sup>25,26</sup>

## ■ ASSOCIATED CONTENT

### SI Supporting Information

The Supporting Information is available free of charge at <https://pubs.acs.org/doi/10.1021/acsinfecdis.0c00501>.

Figure S1: a comparison of the vinyl sulfone inhibitors in the active site of SmCB1; Figure S2: antischistosomal activity, cytotoxicity, and plasma stability of selected vinyl sulfone inhibitors; Figure S3: correlation between the inhibitory potency and the calculated binding energies of the vinyl sulfone inhibitors; Table S1: list of 34 vinyl sulfone inhibitors and their SMILE strings; Table S2: list of contacts formed between SmCB1 and the inhibitors; Table S3: subsite interaction “free” energies between the inhibitors and SmCB1 (PDF)

### Accession Codes

Atomic coordinates and experimental structure factors have been deposited in the Protein Data Bank with accession codes SOGR and SOGQ for SmCB1-WRR-286 and SmCB1-WRR-391, respectively.

## ■ AUTHOR INFORMATION

### Corresponding Author

Michael Mareš – Institute of Organic Chemistry and Biochemistry, Czech Academy of Sciences, 16610 Prague, Czech Republic; Email: [mares@uochb.cas.cz](mailto:mares@uochb.cas.cz)

### Authors

Adéla Jílková – Institute of Organic Chemistry and Biochemistry, Czech Academy of Sciences, 16610 Prague, Czech Republic

Petra Rubešová – Institute of Organic Chemistry and Biochemistry, Czech Academy of Sciences, 16610 Prague, Czech Republic

Jindřich Fanfrlík – Institute of Organic Chemistry and Biochemistry, Czech Academy of Sciences, 16610 Prague, Czech Republic

Pavla Fajtová – Institute of Organic Chemistry and Biochemistry, Czech Academy of Sciences, 16610 Prague, Czech Republic

Pavlna Řezáčová – Institute of Organic Chemistry and Biochemistry, Czech Academy of Sciences, 16610 Prague, Czech Republic

Jiří Brynda – Institute of Organic Chemistry and Biochemistry, Czech Academy of Sciences, 16610 Prague, Czech Republic

Martin Lepšík – Institute of Organic Chemistry and Biochemistry, Czech Academy of Sciences, 16610 Prague, Czech Republic; [orcid.org/0000-0003-2607-8132](https://orcid.org/0000-0003-2607-8132)

Helena Mertlíková-Kaiserová – Institute of Organic Chemistry and Biochemistry, Czech Academy of Sciences, 16610 Prague, Czech Republic

Cory D. Emal – Eastern Michigan University, Ypsilanti, Michigan 48197, United States

Adam R. Renslo – University of California San Francisco, San Francisco, California 94143, United States; [orcid.org/0000-0002-1240-2846](https://orcid.org/0000-0002-1240-2846)

William R. Roush – The Scripps Research Institute, Jupiter, Florida 33458, United States; [orcid.org/0000-0001-9785-5897](https://orcid.org/0000-0001-9785-5897)

Martin Horn – Institute of Organic Chemistry and Biochemistry, Czech Academy of Sciences, 16610 Prague, Czech Republic; [orcid.org/0000-0001-9110-2018](https://orcid.org/0000-0001-9110-2018)

Conor R. Caffrey – Center for Discovery and Innovation in Parasitic Diseases, Skaggs School of Pharmacy and Pharmaceutical Sciences, University of California San Diego, La Jolla, California 92093, United States

Complete contact information is available at: <https://pubs.acs.org/doi/10.1021/acsinfecdis.0c00501>

### Notes

The authors declare no competing financial interest.

## ■ ACKNOWLEDGMENTS

This work was supported by grants LTAUSA19109 and LH15040, project InterBioMed LO1302 from the Ministry of Education of the Czech Republic, grant NV18-05-00345 from the Ministry of Health of the Czech Republic, project ChemBioDrug CZ.02.1.01/0.0/0.0/16\_019/0000729 from the European Regional Development Fund (OP RDE), and the institutional project RVO 61388963. P.R. and J.B. were supported by project LO1304 from the Ministry of Education of the Czech Republic. M.L. and J.F. were also supported by project IT4Innovations National Supercomputing Center - LM2015070 from the Ministry of Education of the Czech Republic. Parasite screens were supported in part by NIH-NIAID R21AI126296 and OPP1171488 from the Bill and Melinda Gates Foundation to C.R.C. We thank Lucie Marešová, Květoslava Kertisová, Martin Svoboda, and Radko Souček (IOCB) for the inhibitor analysis. We also thank Petr Páchl (IOCB) and Brian Suzuki (CDIPD) for support in crystallography and the parasite screens, respectively. Diffraction data were collected on MX14.1 at the BESSY II electron storage ring operated by the Helmholtz-Zentrum Berlin.

## ■ ABBREVIATIONS

AMC, aminomethylcoumarin; Bn, benzyl; Cbz, benzyloxycarbonyl; Et-Pipd, ethyl 1-formylpiperidine-4-carboxylate; Hph, homophenylalanine; HuCB, human cathepsin B; Me-Pipz, N-methylpiperazinylcarbonyl; NTS, newly transformed schistosomula; RMSD, root-mean-square deviation; SmCB1, cathepsin B1 from *Schistosoma mansoni*

## ■ REFERENCES

- (1) Colley, D. G., Bustinduy, A. L., Secor, W. E., and King, C. H. (2014) Human schistosomiasis. *Lancet* 383 (9936), 2253–2264.
- (2) Burke, M. L., Jones, M. K., Gobert, G. N., Li, Y. S., Ellis, M. K., and McManus, D. P. (2009) Immunopathogenesis of human schistosomiasis. *Parasite Immunol.* 31 (4), 163–176.
- (3) Caffrey, C. R. (2007) Chemotherapy of schistosomiasis: present and future. *Curr. Opin. Chem. Biol.* 11 (4), 433–439.
- (4) Caffrey, C. R., and Secor, W. E. (2011) Schistosomiasis: from drug deployment to drug development. *Curr. Opin. Infect. Dis.* 24 (5), 410–417.
- (5) Thetiot-Laurent, S. A., Boissier, J., Robert, A., and Meunier, B. (2013) Schistosomiasis chemotherapy. *Angew. Chem., Int. Ed.* 52 (31), 7936–7956.
- (6) Delcroix, M., Sajid, M., Caffrey, C. R., Lim, K. C., Dvořák, J., Hsieh, I., Bahgat, M., Dissous, C., and McKerrow, J. H. (2006) A multienzyme network functions in intestinal protein digestion by a platyhelminth parasite. *J. Biol. Chem.* 281 (51), 39316–39329.
- (7) Caffrey, C. R., Goupil, L., Rebello, K. M., Dalton, J. P., and Smith, D. (2018) Cysteine proteases as digestive enzymes in parasitic helminths. *PLoS Neglected Trop. Dis.* 12 (8), e0005840.

- (8) Caffrey, C. R., and Ruppel, A. (1997) Cathepsin B-like activity predominates over cathepsin L-like activity in adult *Schistosoma mansoni* and *S. japonicum*. *Parasitol. Res.* 83 (6), 632–635.
- (9) Sajid, M., McKerrow, J. H., Hansell, E., Mathieu, M. A., Lucas, K. D., Hsieh, I., Greenbaum, D., Bogyo, M., Salter, J. P., Lim, K. C., Franklin, C., Kim, J. H., and Caffrey, C. R. (2003) Functional expression and characterization of *Schistosoma mansoni* cathepsin B and its trans-activation by an endogenous asparaginyl endopeptidase. *Mol. Biochem. Parasitol.* 131 (1), 65–75.
- (10) Jílková, A., Řezáčová, P., Lepšík, M., Horn, M., Váchová, J., Fanfrlík, J., Brynda, J., McKerrow, J. H., Caffrey, C. R., and Mareš, M. (2011) Structural basis for inhibition of cathepsin B drug target from the human blood fluke, *Schistosoma mansoni*. *J. Biol. Chem.* 286 (41), 35770–35781.
- (11) Musil, D., Zucic, D., Turk, D., Engh, R. A., Mayr, I., Huber, R., Popovic, T., Turk, V., Towatari, T., and Katunuma, N. (1991) The refined 2.15 Å X-ray crystal structure of human liver cathepsin B: the structural basis for its specificity. *EMBO J.* 10 (9), 2321–2330.
- (12) Jílková, A., Horn, M., Řezáčová, P., Marešová, L., Fajtová, P., Brynda, J., Vondrášek, J., McKerrow, J. H., Caffrey, C. R., and Mareš, M. (2014) Activation Route of the *Schistosoma mansoni* Cathepsin B1 Drug Target: Structural Map with a Glycosaminoglycan Switch. *Structure* 22 (12), 1786–1798.
- (13) Abdulla, M. H., Lim, K. C., Sajid, M., McKerrow, J. H., and Caffrey, C. R. (2007) Schistosomiasis mansoni: novel chemotherapy using a cysteine protease inhibitor. *PLoS Med.* 4 (1), e14.
- (14) Palmer, J. T., Rasnick, D., Klaus, J. L., and Brömme, D. (1995) Vinyl sulfones as mechanism-based cysteine protease inhibitors. *J. Med. Chem.* 38 (17), 3193–3196.
- (15) Brömme, D., Klaus, J. L., Okamoto, K., Rasnick, D., and Palmer, J. T. (1996) Peptidyl vinyl sulphones: a new class of potent and selective cysteine protease inhibitors: S2P2 specificity of human cathepsin O2 in comparison with cathepsins S and L. *Biochem. J.* 315 (1), 85–89.
- (16) Marco, M., and Coteron, J. M. (2012) Falcipain inhibition as a promising antimalarial target. *Curr. Top. Med. Chem.* 12 (5), 408–444.
- (17) Steverding, D., Caffrey, C. R., and Sajid, M. (2006) Cysteine proteinase inhibitors as therapy for parasitic diseases: advances in inhibitor design. *Mini-Rev. Med. Chem.* 6 (9), 1025–1032.
- (18) Engel, J. C., Doyle, P. S., Hsieh, I., and McKerrow, J. H. (1998) Cysteine protease inhibitors cure an experimental *Trypanosoma cruzi* infection. *J. Exp. Med.* 188 (4), 725–734.
- (19) Vermeire, J. J., Lantz, L. D., and Caffrey, C. R. (2012) Cure of hookworm infection with a cysteine protease inhibitor. *PLoS Neglected Trop. Dis.* 6 (7), e1680.
- (20) Shenai, B. R., Lee, B. J., Alvarez-Hernandez, A., Chong, P. Y., Emal, C. D., Neitz, R. J., Roush, W. R., and Rosenthal, P. J. (2003) Structure-activity relationships for inhibition of cysteine protease activity and development of *Plasmodium falciparum* by peptidyl vinyl sulfones. *Antimicrob. Agents Chemother.* 47 (1), 154–60.
- (21) Powers, J. C., Asgian, J. L., Ekici, O. D., and James, K. E. (2002) Irreversible inhibitors of serine, cysteine, and threonine proteases. *Chem. Rev.* 102 (12), 4639–750.
- (22) Sajid, M., Robertson, S. A., Brinen, L. S., and McKerrow, J. H. (2011) Cruzain: the path from target validation to the clinic. *Adv. Exp. Med. Biol.* 712, 100–15.
- (23) McKerrow, J. H. (2018) Update on drug development targeting parasite cysteine proteases. *PLoS Neglected Trop. Dis.* 12 (8), e0005850.
- (24) Betts, M. J., and Sternberg, M. J. (1999) An analysis of conformational changes on enzyme-protein association: implications for predictive docking. *Protein Eng., Des. Sel.* 12 (4), 271–83.
- (25) Long, T., Neitz, R. J., Beasley, R., Kalyanaraman, C., Suzuki, B. M., Jacobson, M. P., Dissous, C., McKerrow, J. H., Drewry, D. H., Zuercher, W. J., Singh, R., and Caffrey, C. R. (2016) Structure-Bioactivity Relationship for Benzimidazole Thiophene Inhibitors of Polo-Like Kinase 1 (PLK1), a Potential Drug Target in *Schistosoma mansoni*. *PLoS Neglected Trop. Dis.* 10 (1), e0004356.
- (26) Glaser, J., Schurig, U., Suzuki, B. M., Caffrey, C. R., and Holzgrabe, U. (2015) Anti-Schistosomal Activity of Cinnamic Acid Esters: Eugenyl and Thymyl Cinnamate Induce Cytoplasmic Vacuoles and Death in Schistosomula of *Schistosoma mansoni*. *Molecules* 20 (6), 10873–10883.
- (27) Wendt, G., Zhao, L., Chen, R., Liu, C., O'Donoghue, A. J., Caffrey, C. R., Reese, M. L., and Collins, J. J., 3rd. (2020) A single-cell RNA-seq atlas of *Schistosoma mansoni* identifies a key regulator of blood feeding. *Science* 369 (6511), 1644–1649.
- (28) Correnti, J. M., Brindley, P. J., and Pearce, E. J. (2005) Long-term suppression of cathepsin B levels by RNA interference retards schistosome growth. *Mol. Biochem. Parasitol.* 143 (2), 209–15.
- (29) Fonseca, N. C., da Cruz, L. F., da Silva Villela, F., do Nascimento Pereira, G. A., de Siqueira-Neto, J. L., Kellar, D., Suzuki, B. M., Ray, D., de Souza, T. B., Alves, R. J., Sales Junior, P. A., Romanha, A. J., Murta, S. M., McKerrow, J. H., Caffrey, C. R., de Oliveira, R. B., and Ferreira, R. S. (2015) Synthesis of a sugar-based thiosemicarbazone series and structure-activity relationship versus the parasite cysteine proteases rhodesain, cruzain, and *Schistosoma mansoni* cathepsin B1. *Antimicrob. Agents Chemother.* 59 (5), 2666–2677.
- (30) Lopes, M. S., Suzuki, B. M., Pereira, G. A. d. N., Probst, A. C., Ferreira, R. S., Oliveira, J. T. d., Tecchio, K. B., Santos, F. V. d., Caffrey, C. R., and Oliveira, R. B. d. (2018) Ortho-nitrobenzyl derivatives as potential anti-schistosomal agents. *Brazilian Journal of Pharmaceutical Sciences* 54, 1.
- (31) Choe, Y., Leonetti, F., Greenbaum, D. C., Lecaille, F., Bogyo, M., Brömme, D., Ellman, J. A., and Craik, C. S. (2006) Substrate profiling of cysteine proteases using a combinatorial peptide library identifies functionally unique specificities. *J. Biol. Chem.* 281 (18), 12824–12832.
- (32) Turk, V., Stoka, V., Vasiljeva, O., Renko, M., Sun, T., Turk, B., and Turk, D. (2012) Cysteine cathepsins: from structure, function and regulation to new frontiers. *Biochim. Biophys. Acta, Proteins Proteomics* 1824 (1), 68–88.
- (33) Kerr, I. D., Lee, J. H., Farady, C. J., Marion, R., Rickert, M., Sajid, M., Pandey, K. C., Caffrey, C. R., Legac, J., Hansell, E., McKerrow, J. H., Craik, C. S., Rosenthal, P. J., and Brinen, L. S. (2009) Vinyl sulfones as antiparasitic agents and a structural basis for drug design. *J. Biol. Chem.* 284 (38), 25697–25703.
- (34) Brinen, L. S., Hansell, E., Cheng, J., Roush, W. R., McKerrow, J. H., and Fletterick, R. J. (2000) A target within the target: probing cruzain's P1' site to define structural determinants for the Chagas' disease protease. *Structure* 8 (8), 831–840.
- (35) Abdulla, M. H., Ruelas, D. S., Wolff, B., Snedecor, J., Lim, K. C., Xu, F., Renslo, A. R., Williams, J., McKerrow, J. H., and Caffrey, C. R. (2009) Drug discovery for schistosomiasis: hit and lead compounds identified in a library of known drugs by medium-throughput phenotypic screening. *PLoS Neglected Trop. Dis.* 3 (7), e478.
- (36) Caffrey, C. R., Hansell, E., Lucas, K. D., Brinen, L. S., Alvarez, H. A., Cheng, J., Gwaltney, S. L., Roush, W. R., Stierhof, Y. D., Bogyo, M., Steverding, D., and McKerrow, J. H. (2001) Active site mapping, biochemical properties and subcellular localization of rhodesain, the major cysteine protease of *Trypanosoma brucei rhodesiense*. *Mol. Biochem. Parasitol.* 118 (1), 61–73.
- (37) Roush, W. R., Gwaltney, S. L., Cheng, J., Scheidt, K. A., McKerrow, J. H., and Hansell, E. (1998) Vinyl Sulfonate Esters and Vinyl Sulfonamides: Potent, Irreversible Inhibitors of Cysteine Proteases. *J. Am. Chem. Soc.* 120 (42), 10994–10995.
- (38) Roush, W. R., Cheng, J., Knapp-Reed, B., Alvarez-Hernandez, A., McKerrow, J. H., Hansell, E., and Engel, J. C. (2001) Potent second generation vinyl sulfonamide inhibitors of the trypanosomal cysteine protease cruzain. *Bioorg. Med. Chem. Lett.* 11 (20), 2759–2762.
- (39) Ang, K. K., Ratnam, J., Gut, J., Legac, J., Hansell, E., Mackey, Z. B., Skrzypczynska, K. M., Debnath, A., Engel, J. C., Rosenthal, P. J., McKerrow, J. H., Arkin, M. R., and Renslo, A. R. (2011) Mining a cathepsin inhibitor library for new antiparasitic drug leads. *PLoS Neglected Trop. Dis.* 5 (5), e1023.



- (40) Reddick, J. J., Cheng, J., and Roush, W. R. (2003) Relative rates of Michael reactions of 2'-(phenethyl)thiol with vinyl sulfones, vinyl sulfonate esters, and vinyl sulfonamides relevant to vinyl sulfonyl cysteine protease inhibitors. *Org. Lett.* 5 (11), 1967–70.
- (41) Somoza, J. R., Zhan, H., Bowman, K. K., Yu, L., Mortara, K. D., Palmer, J. T., Clark, J. M., and McGrath, M. E. (2000) Crystal structure of human cathepsin V. *Biochemistry* 39 (41), 12543–12551.
- (42) Baell, J. B., and Holloway, G. A. (2010) New Substructure Filters for Removal of Pan Assay Interference Compounds (PAINS) from Screening Libraries and for Their Exclusion in Bioassays. *J. Med. Chem.* 53 (7), 2719–2740.
- (43) Horn, M., Jílková, A., Vondrášek, J., Marešová, L., Caffrey, C. R., and Mareš, M. (2011) Mapping the Pro-Peptide of the *Schistosoma mansoni* Cathepsin B1 Drug Target: Modulation of Inhibition by Heparin and Design of Mimetic Inhibitors. *ACS Chem. Biol.* 6 (6), 609–617.
- (44) Jílková, A., Horn, M., and Mareš, M. (2020) Structural and Functional Characterization of *Schistosoma mansoni* Cathepsin B1. *Methods Mol. Biol.* 2151, 145–158.
- (45) Mueller, U., Förster, R., Hellmig, M., Huschmann, F. U., Kastner, A., Malecki, P., Pühringer, S., Röwer, M., Sparta, K., Steffien, M., Ühlein, M., Wilk, P., and Weiss, M. S. (2015) The macromolecular crystallography beamlines at BESSY II of the Helmholtz-Zentrum Berlin: Current status and perspectives. *Eur. Phys. J. Plus* 130 (7), 141.
- (46) Kabsch, W. (2010) Xds. *Acta Crystallogr., Sect. D: Biol. Crystallogr.* 66 (2), 125–32.
- (47) Karpplus, P. A., and Diederichs, K. (2012) Linking crystallographic model and data quality. *Science* 336 (6084), 1030–3.
- (48) Brünger, A. T. (1992) Free R value: a novel statistical quantity for assessing the accuracy of crystal structures. *Nature* 355 (6359), 472–475.
- (49) Lovell, S. C., Davis, I. W., Arendall, W. B., III, de Bakker, P. I., Word, J. M., Prisant, M. G., Richardson, J. S., and Richardson, D. C. (2003) Structure validation by C $\alpha$  geometry: phi, psi and Cbeta deviation. *Proteins: Struct., Funct., Genet.* 50 (3), 437–450.
- (50) Vagin, A., and Teplyakov, A. (2000) An approach to multi-copy search in molecular replacement. *Acta Crystallogr., Sect. D: Biol. Crystallogr.* 56 (12), 1622–1624.
- (51) Murshudov, G. N., Vagin, A. A., and Dodson, E. J. (1997) Refinement of macromolecular structures by the maximum-likelihood method. *Acta Crystallogr., Sect. D: Biol. Crystallogr.* 53 (3), 240–255.
- (52) Winn, M. D., Ballard, C. C., Cowtan, K. D., Dodson, E. J., Emsley, P., Evans, P. R., Keegan, R. M., Krissinel, E. B., Leslie, A. G., McCoy, A., McNicholas, S. J., Murshudov, G. N., Pannu, N. S., Potterton, E. A., Powell, H. R., Read, R. J., Vagin, A., and Wilson, K. S. (2011) Overview of the CCP4 suite and current developments. *Acta Crystallogr., Sect. D: Biol. Crystallogr.* 67 (4), 235–242.
- (53) Emsley, P., and Cowtan, K. (2004) Coot: model-building tools for molecular graphics. *Acta Crystallogr., Sect. D: Biol. Crystallogr.* 60 (12), 2126–2132.
- (54) Hostaš, J., and Řezáč, J. (2017) Accurate DFT-D3 Calculations in a Small Basis Set. *J. Chem. Theory Comput.* 13 (8), 3575–3585.
- (55) Klamt, A., and Schuurmann, G. (1993) Cosmo - a New Approach to Dielectric Screening in Solvents with Explicit Expressions for the Screening Energy and Its Gradient. *J. Chem. Soc., Perkin Trans. 2* 2 (5), 799–805.
- (56) Ahlrichs, R., Bar, M., Haser, M., Horn, H., and Kolmel, C. (1989) Electronic-Structure Calculations on Workstation Computers - the Program System Turbomole. *Chem. Phys. Lett.* 162 (3), 165–169.
- (57) Řezáč, J. (2016) Cuby: An integrative framework for computational chemistry. *J. Comput. Chem.* 37 (13), 1230–7.
- (58) Winn, M. D., Isupov, M. N., and Murshudov, G. N. (2001) Use of TLS parameters to model anisotropic displacements in macromolecular refinement. *Acta Crystallogr., Sect. D: Biol. Crystallogr.* 57 (1), 122–133.
- (59) Salentin, S., Schreiber, S., Haupt, V. J., Adasme, M. F., and Schroeder, M. (2015) PLIP: fully automated protein-ligand interaction profiler. *Nucleic Acids Res.* 43 (W1), W443–W447.
- (60) Case, D. A., Darden, T. A., Cheatham, I. T. E., Simmerling, C. L., Wang, J., Duke, R. E., Luo, R., Crowley, M., Walker, R. C., Zhang, W., Merz, K. M., Wang, B., Hayik, S., Roitberg, A., Seabra, G., Kolossváry, I., Wong, K. F., Paesani, F., Vanicek, J., Wu, X., Brozell, S. R., Steinbrecher, T., Gohlke, H., Yang, L., Tan, C., Mongan, J., Hornak, V., Cui, G., Mathews, D. H., Seetin, M. G., Sagui, C., Babin, V., and Kollman, P. A. (2008) AMBER 10, University of California, San Francisco.
- (61) Řezáč, J., and Hobza, P. (2012) Advanced Corrections of Hydrogen Bonding and Dispersion for Semiempirical Quantum Mechanical Methods. *J. Chem. Theory Comput.* 8 (1), 141–51.
- (62) Stewart, J. J. P. (2016) MOPAC2016, Stewart Computational Chemistry, Colorado Springs.
- (63) Vorlová, B., Nachtigallová, D., Jirásková-Vaničková, J., Ajani, H., Jansa, P., Řezáč, J., Fanfrlík, J., Otyepka, M., Hobza, P., Konvalinka, J., and Lepšík, M. (2015) Malonate-based inhibitors of mammalian serine racemase: kinetic characterization and structure-based computational study. *Eur. J. Med. Chem.* 89, 189–97.
- (64) Massova, I., and Kollman, P. A. (1999) Computational alanine scanning to probe protein-protein interactions: A novel approach to evaluate binding free energies. *J. Am. Chem. Soc.* 121 (36), 8133–8143.
- (65) Pecina, A., Lepšík, M., Řezáč, J., Brynda, J., Mader, P., Řezáčová, P., Hobza, P., and Fanfrlík, J. (2013) QM/MM calculations reveal the different nature of the interaction of two carborane-based sulfamide inhibitors of human carbonic anhydrase II. *J. Phys. Chem. B* 117 (50), 16096–104.
- (66) Fanfrlík, J., Brahmkshatriya, P. S., Řezáč, J., Jílková, A., Horn, M., Mareš, M., Hobza, P., and Lepšík, M. (2013) Quantum mechanics-based scoring rationalizes the irreversible inactivation of parasitic *Schistosoma mansoni* cysteine peptidase by vinyl sulfone inhibitors. *J. Phys. Chem. B* 117 (48), 14973–14982.
- (67) Stefanić, S., Dvořák, J., Horn, M., Braschi, S., Sojka, D., Ruelas, D. S., Suzuki, B., Lim, K.-C., Hopkins, S. D., McKerrow, J. H., and Caffrey, C. R. (2010) RNA Interference in *Schistosoma mansoni* Schistosomula: Selectivity, Sensitivity and Operation for Larger-Scale Screening. *PLoS Neglected Trop. Dis.* 4 (10), e850.
- (68) Basch, P. F. (1981) Cultivation of *Schistosoma mansoni* in vitro. I. Establishment of cultures from cercariae and development until pairing. *J. Parasitol.* 67 (2), 179–185.
- (69) Dvořák, J., Fajtová, P., Ulrychová, L., Leontovych, A., Rojo-Arreola, L., Suzuki, B. M., Horn, M., Mareš, M., Craik, C. S., Caffrey, C. R., and O'Donoghue, A. J. (2016) Excretion/secretion products from *Schistosoma mansoni* adults, eggs and schistosomula have unique peptidase specificity profiles. *Biochimie* 122, 99–109.
- (70) Fajtová, P., Stefanić, S., Hradilek, M., Dvořák, J., Vondrášek, J., Jílková, A., Ulrychová, L., McKerrow, J. H., Caffrey, C. R., Mareš, M., and Horn, M. (2015) Prolyl Oligopeptidase from the Blood Fluke *Schistosoma mansoni*: From Functional Analysis to Anti-schistosomal Inhibitors. *PLoS Neglected Trop. Dis.* 9 (6), e0003827.